

## DEPENDENCE OF GALVANOMAGNETIC EFFECTS IN Sb ON TEMPERATURE AND PRESSURE

V. V. KECHIN, A. I. LIKHTER, and Yu. A. POSPELOV

Institute of High Pressure Physics, Academy of Sciences, U.S.S.R.

Submitted to JETP editor January 27, 1965

J. Exptl. Theoret. Phys. (U.S.S.R.) **49**, 36-46 (July, 1965)

The influence of hydrostatic pressure up to 10 000 atm on the twelve galvanomagnetic coefficients at room temperature is investigated. The temperature dependence of the coefficients is measured (at 293°, 273°, 195°, and 77°K) under atmospheric pressure. It is shown that the number of carriers is independent of temperature, but that mobility is proportional to  $T^{-p}$  ( $p = 1.3-1.4$ ). The deformation of the electron Fermi surface by pressure is calculated. It is shown that the carrier concentration decreases under pressure. With increasing pressure the effective-mass anisotropy is enhanced, whereas the tilt of the electron ellipsoids is diminished by about 7° at 10 000 atm.

### 1. INTRODUCTION

ANTIMONY crystallizes in a  $D_{3d}^5$  ( $R\bar{3}m$ ) rhombohedral structure having two atoms in each unit cell; this metal has a low density of charge carriers ( $\sim 10^{-3}$  per atom). Arkhipov<sup>[1]</sup> has shown that the energy spectrum of this type of metal cannot be observed by gradually changing lattice separations and has considered a feasible different procedure. The degeneracy of the energy spectrum of a highly symmetric structure can be lifted if some symmetry elements disappear, leaving a so-called distorted structure having parameters very close to those of the original structure. Abrikosov and Fal'kovskii<sup>[2]</sup> accordingly consider metals of the Bi type as having a distorted primitive cubic structure.

The distortion is characterized by the displacement of the central atom through the distance  $\frac{1}{2} - 2u$  ( $u = 0.233$ ) and by the change of the corner angle  $\alpha$  from 60° (for the cubic structure) to 57°06.5'.<sup>[3]</sup> In hexagonal coordinates this angle corresponds to the ratio  $c/a = 2.62$  instead of 2.45 ( $\sqrt{6}$ ) for the cube. Sb resembles Bi; the two elements have almost identical values of  $u$ ,  $\alpha$ , and  $c/a$ .

The general form of the energy spectrum has been investigated for Bi-type metals; it has been shown that the electron parts of the Fermi surface are located along the binary axes, while the hole part is located at the center of the Brillouin zone.<sup>[2]</sup> The shapes of these parts of the surface depend on the ratio of the theoretical parameters and can be very complex as a general rule.

It has been shown by many experimental studies (in<sup>[4]</sup>, for example) that the electron surface of Bi is approximated well by three ellipsoids, each having one axis along a binary crystal axis and the other tilted  $\theta = 6^\circ$  from the trigonal axis; the hole part is approximated by an ellipsoid of revolution having its principal axis along the trigonal crystal axis. The carrier concentration in Bi is of the order of  $10^{-5}$  per atom. In Si the carrier concentration is greater by two orders of magnitude and the electron Fermi surface is well described by the ellipsoid model (with  $\sim 36^\circ$  tilt).<sup>[5]</sup> The shape of the hole Fermi surface has still not been determined conclusively. Data on cyclotron resonance and oscillatory effects<sup>[6]</sup> can apparently be accounted for by the existence of a few hole zones at the coordinate origin.

The difference between the structure of Sb (or Bi) and a simple cubic lattice decreases gradually as the pressure is increased to a high level. It follows from Bridgman's measurements of the linear compressibility of Bi and Sb along the  $c$  and  $a$  axes (in hexagonal coordinates) up to 12 000 atm,<sup>[7]</sup> that  $c/a$  diminishes with increasing pressure, while the angle  $\alpha$  approaches 60°, increasing by 24' at 10 000 atm. In Bi this gradual progress toward the cubic structure is interrupted by known transformations, to modification II at 25 400 atm and to modification III at 26 900 atm. Bi is then no longer a metal with a small carrier concentration.<sup>[8]</sup> The x-ray studies of Vereshchagin and Kabalkina<sup>[9]</sup> have shown that the gradual removal of the "distortions" in Bi leads to a simple cubic structure at about 70 000 atm. The reduction of the

ratio  $c/a$  was traced up to 50 000 atm; the form of the pressure dependence of  $u$  remains undetermined.

It was shown in<sup>[2]</sup> that the parameters of the energy spectrum of carriers in Bi-type metals are determined from the values of  $u$  and  $c/a$ . It was the principal purpose of the present work to investigate the variation of the Sb energy spectrum, accompanying a gradual reduction of  $c/a$  and of the angle difference  $60^\circ - \alpha$  under high hydrostatic pressures.

## 2. EXPERIMENT

Using our previously designed apparatus,<sup>[10]</sup> we measured the components of the resistivity tensor of Sb single crystals in a magnetic field. These crystals were grown from Su-000 antimony<sup>1)</sup> by zone melting in a helium atmosphere that reduced Sb evaporation considerably. Each grown single crystal was cleaved in the (111) plane and was then cut with a spark cutter into plates 8–10 mm long with  $0.3 \times (1.5-2)$ -mm<sup>2</sup> cross sections in directions permitting the measurement of all resistivity tensor components in a magnetic field.<sup>[11]</sup> The samples were etched in a  $\text{FeCl}_3 + \text{HCl} + \text{H}_2\text{O}$  mixture (1 : 3 : 12) before contacts were soldered on them.<sup>2)</sup> The samples were then mounted in a plastic holder on the face of the pressure-vessel obturator. This vessel was positioned at the center of the gap of a magnet that could be rotated horizontally. The samples could therefore be oriented according to the Hall emf and magnetoresistance rosettes. The total error incurred in cutting and orienting was not greater than 2–3°.

The samples were not cemented, but were inserted into narrow slots in the holder in order to obviate any uniaxial stresses resulting from higher pressures. The rosettes recorded under pressure showed that the positions of the samples had not changed; this is also indicated by the complete reversibility of the pressure-dependent effects. The pressure dependence of galvanomagnetic effects was measured at room temperature under benzine up to 10 000 atm. The temperature dependences of the galvanomagnetic coefficients were measured without a pressure increase at room temperature (293°K) in three different media:

<sup>1)</sup>The original material contained the following certified percentages of impurities: Sn  $< 8 \times 10^{-5}$ ; Cu  $< 3 \times 10^{-5}$ ; Ag  $< 5 \times 10^{-5}$ ; Bi  $< 6 \times 10^{-5}$ ; Ni  $< 2 \times 10^{-4}$ ; Pb  $< 2 \times 10^{-4}$ ; As  $< 5 \times 10^{-4}$ ; Fe  $< 4 \times 10^{-4}$ .

<sup>2)</sup>The authors are indebted to T. D. Varfolomeev for growing and cutting the Sb single crystals.

melting ice (273°K), solid carbon dioxide mixed with ethyl alcohol (195°K), and liquid nitrogen (77.3°K). The dc potentiometer circuit used for these measurements had  $3 \times 10^{-8}$  V sensitivity.

## 3. DETERMINATION OF THE RESISTIVITY TENSOR COMPONENTS IN A MAGNETIC FIELD

It follows from symmetry considerations<sup>[11]</sup> that Sb has two resistivity components  $\rho_{11}$  and  $\rho_{33}$ , two Hall coefficients  $R_{231}$  and  $R_{123}$ , and eight magnetoresistance components  $A_{11}(\rho_{11,11})$ ,  $A_{12}(\rho_{11,22})$ ,  $A_{13}(\rho_{11,33})$ ,  $A_{31}(\rho_{33,11})$ ,  $A_{44}(\rho_{23,23})$ ,  $A_{24}(\rho_{22,23})$ ,  $A_{33}(\rho_{33,33})$ , and  $A_{42}(\rho_{23,22})$ .

To determine  $R_{231}$  and  $R_{123}$  the measured values of the Hall emf  $E$  were averaged for two mutually perpendicular field directions, were divided by the magnetic field strength  $H$ , and were then plotted as a function of  $H^2$ . By extrapolating the linear part of the curve to the ordinate axis we obtain  $\lim(E/H)$  for  $H \rightarrow 0$ . Dividing this quantity by the current  $J$  passed through the plate and multiplying by its thickness  $t$ , we obtain the absolute value of  $R_{ijk}$ .

To determine the coefficients  $A_{ij}$ , the mean difference  $E(H) - E(0)$  of potential drops in the resistance of a crystal was divided by  $H^2$ ; the result was then plotted as a function of  $H^2$ . The ordinate intercept gives  $\lim\{[E(H) - E(0)]/H^2\}$  for  $H \rightarrow 0$ . Dividing this quantity by  $J$  and multiplying by  $at/l$ , where  $a$  is the width of the Sb plate and  $l$  is the separation of the potential contacts, we obtain the absolute value of  $A_{ij}$ . The difference between the values of  $E(H) - E(0)$  for two mutually perpendicular field directions is of the order of the measurement error.

In determining the pressure dependences of  $\rho_{ij}$ ,  $R_{ijk}$ , and  $A_{ij}$ , the values of  $a$ ,  $t$ , and  $l$  were corrected for the linear compressibility.<sup>[7]</sup> At room temperature the linear dependences of  $E/H$  and  $\Delta E/H^2$  on  $H^2$  continue up to at least 10 kOe; at 77.3°K linear dependence is observed only up to  $\sim 3$  kOe.

## 4. EXPERIMENTAL RESULTS

Table I shows the measured resistivity tensor components in a magnetic field at four different temperatures. The indicated error limits were calculated from the spread of values for 22 samples. At room temperature  $\rho_{11}$  and  $\rho_{33}$  were measured for 10 samples; the other coefficients were measured for four or five samples. Our values of  $\rho_{ij}$ ,  $R_{ijk}$ , and  $A_{ij}$  were compared with the results given in<sup>[12,13]</sup>. In<sup>[12]</sup> the crystal plates were cut, as in our case, from a large single crystal; in<sup>[13]</sup>

Table I. Resistivity tensor components in a magnetic field versus temperature

T, °K	Resistivity components, 10 <sup>-5</sup> ohm-cm		Hall coefficients, 10 <sup>-7</sup> ohm-cm-kOe <sup>-1</sup>		Magnetoresistance components, 10 <sup>-9</sup> ohm-cm-kOe <sup>-2</sup>							
	$\rho_{11}$	$\rho_{33}$	$-R_{231}$	$-R_{123}$	$A_{12}$	$A_{13}$	$A_{31}$	$A_{31}$	$A_{33}$	$-A_{44}$	$-A_{24}$	$-A_{42}$
293 [12]	4.3	3.64	2.2	2.51	19.9	6.4	13.6	7.3	5.2	2.8	3.5	1.4
293 [13]	4.43	3.46	2.05	2.34	16.5	5.1	10.8	6.6	2.0	1.5	2.6	2.1
293	4.36	3.62	2.46	2.54	18.2	6.1	15.1	6.5	2.6	1.7	3.0	2.3
273	3.92	3.32	2.48	2.69	19.7	6.8	17.1	6.9	2.9	1.9	3.2	2.5
195	2.60	2.08	2.83	3.07	37.2	13.9	26.4	12.3	4.8	3.1	5.9	4.1
77	0.692	0.557	2.46	3.66	109.5	46.7	69.5	40.1	17.7	11.7	21.0	12.3
Error, %	10	15	10	10	10	15	5	25	20	20	20	20

the samples were grown in the form of rods having the required dimensions and specified orientation. Most of our values lie between the results obtained in the aforesaid two investigations.

Table II shows the temperature dependence of  $\rho_{11}$  for two samples. The spread of the relative values is 2–3%, whereas the absolute values differ by almost 10%. A similar pattern is observed in the temperature dependences of all other resistivity tensor components.

Table II. Resistivity versus temperature for two Sb samples

T, °K	$\rho_{11}$ , 10 <sup>-5</sup> ohm-cm		$\rho_{11}(T)/\rho_{11}(293^\circ\text{K})$	
	№ 1	№ 2	№ 1	№ 2
293	4.85	4.42	1.000	1.000
273	4.30	4.01	0.886	0.907
195	2.84	2.67	0.585	0.604
77	0.765	0.702	0.0158	0.0159

The resistivity tensor components  $\rho$ , R, and A in a magnetic field were used to calculate the conductivity tensor components  $\sigma$ , P, and B by means of well-known formulas.<sup>[11]</sup> We know that  $B \sim n\mu^3$ , where n is the carrier concentration and  $\mu^3$  is a homogeneous third-degree polynomial in the hole and electron mobility components; these combinations vary for different values of B. The experimental plots of log B vs. log T are straight lines having almost identical slopes (for all B) lying in the narrow range 3.9–4.2; i.e.,  $\mu \sim T^{-p}$ , where  $p = 1.3$ – $1.4$ . Thus all mobility components exhibit identical temperature dependences. Since  $\sigma \sim n\mu$ , all possible combinations of the form  $(\sigma^3/B)^{1/2} \sim n$  should have an identical temperature dependence. This has been confirmed experimentally.

Figure 1 shows the dependence on T (averaged over all samples) of a quantity proportional to the

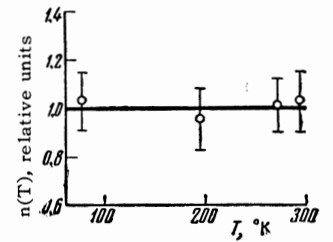


FIG. 1. Carrier density versus temperature.

carrier density n, which is seen to be independent of T within the experimental spread of values. This is consistent with Shoenberg's value of 1300°K for the electron degeneracy temperature of Sb.<sup>[5]</sup>

Figures 2–4 show the pressure dependences, in relative units, of  $\rho_{ij}$ ,  $R_{ijk}$ , and  $A_{ij}$ . In each graph the different symbols pertain to different samples. The galvanomagnetic coefficients, such as the resistivities  $\rho_{11}$  and  $\rho_{33}$ , the Hall coefficients  $R_{123}$  and  $R_{231}$ , and the transverse magnetoresistances  $A_{31}$  and  $A_{12}$ , exhibit highly anisotropic behavior under pressure. While the absolute values of the coefficients have spreads up to 30%, their pressure dependences are determined with considerably greater accuracy (2–5%).

## 5. RELATION OF CONDUCTIVITY TENSOR COMPONENTS TO ENERGY SPECTRUM PARAMETERS OF Sb

To calculate the conductivity tensor components of Sb we represented these, as is customary, in terms of the mobilities  $\mu_i$  in the directions of the ellipsoidal principal axes. Also  $\mu_i = e\tau_i/m_i$ , where  $\tau_i$  and  $m_i$  are the components of the relaxation time and effective mass tensors, respectively.

We shall hereafter use the method proposed in<sup>[14]</sup>. If the hole Fermi surface of Bi-type metals has the symmetry elements derived from the theory of Abrikosov and Fal'kovskii<sup>[2]</sup> (the  $k_z$  axis is the axis of rotation and the  $k_x0k_y$  plane is a mirror

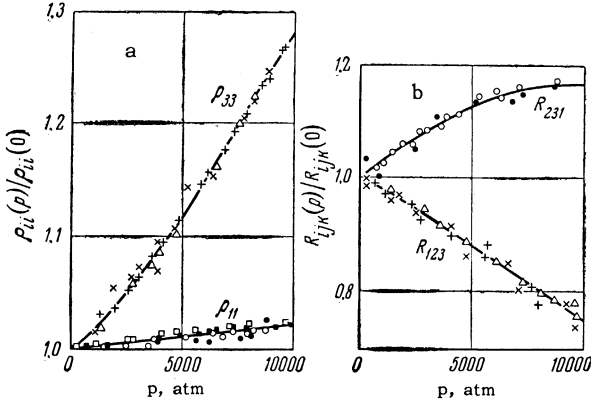


FIG. 2. Pressure dependence of a - resistivity, b - Hall coefficient of Sb.

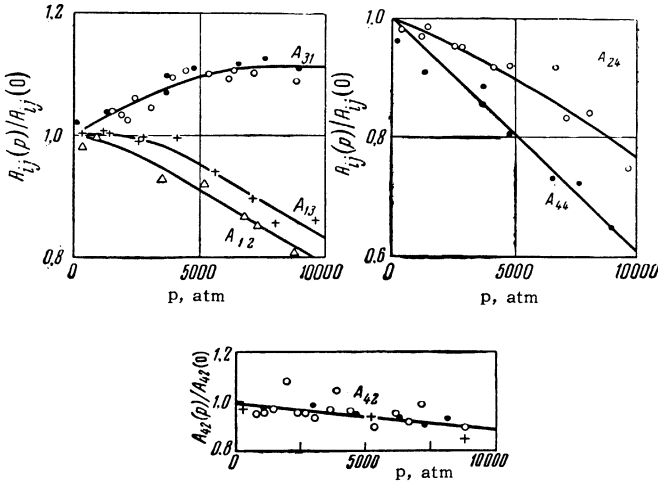


FIG. 3. Pressure dependences of Sb magnetoresistance coefficients.

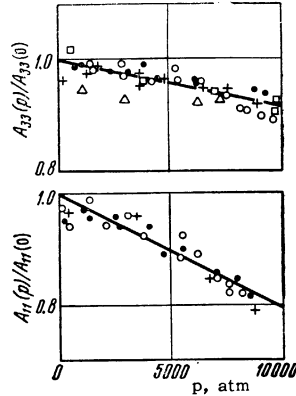


FIG. 4. Pressure dependence of Sb longitudinal magnetoresistance coefficients.

plane), then only the electron mobilities appear in the conductivity tensor components  $B_{33}$ ,  $B_{24}$ , and  $B_{42}$ .

For an arbitrary magnetic field along the trigonal axis direction the expression for the conductivity is

$$\frac{H_3^2}{\sigma_{33}(0) - \sigma_{33}(H_3)} = \frac{1}{B_{33}}(1 + \beta_{33}H_3^2), \quad (1)$$

where

$$\frac{H_3^2}{|\Delta\sigma_{33}(H_3)|} \equiv \frac{H_3^2}{1/\rho_{33}(0) - 1/\rho_{33}(H_3)}. \quad (1a)$$

The formula for the coefficient  $\beta_{33}$  contains only the parameters of the electron Fermi surface.

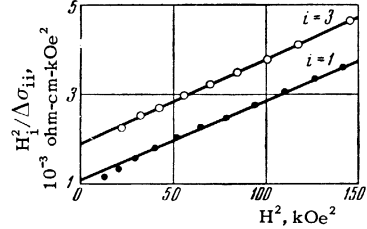


FIG. 5.  $H_3^2/\Delta\sigma_{33}$  versus magnetic field.

Figure 5 shows the dependence of  $H_3^2/\Delta\sigma_{33}(H_3)$  on  $H_3^2$  at 77.3°K up to 12 kOe. The linearity with respect to  $H^2$  is maintained in magnetic fields considerably higher than the saturation field. An analogous graph is shown for the longitudinal magnetoresistance along the binary axis; linearity with respect to  $H^2$  appears here also in the entire magnetic field range. This shows that within the limits of experimental error a valid formula for  $\sigma_{11}(H)$  is analogous to (1):

$$\frac{H_1^2}{|\Delta\sigma_{11}(H_1)|} = \frac{1}{B_{11}}(1 + \beta_{11}H_1^2), \quad (2)$$

where

$$\frac{H_1^2}{|\Delta\sigma_{11}(H_1)|} \equiv \frac{H_1^2}{1/\rho_{11}(0) - 1/\rho_{11}(H_1)}. \quad (2a)$$

The experimentally determined equation (2) can be accounted for by one of the following hypotheses: 1) Within the limits of experimental accuracy  $B_{11}$  and  $\beta_{11}$  depend only on the parameters of the electron Fermi surface; 2) the saturation fields for electrons and poles coincide accidentally. If the first of these two hypotheses is correct, the following relationship exists between the components  $B_{11}$ ,  $B_{33}$ ,  $B_{42}$ , and  $B_{24}$ :

$$2B_{11} = B_{33} + \frac{4B_{24}B_{42}}{B_{33}}; \quad (3)$$

here  $B_{11}$  is determined by quantities depending only on the parameters of the electron Fermi surface. Within experimental accuracy limits (3) is well obeyed at all temperatures and pressures. The experimental pressure dependences of  $\beta_{11}$  and  $\beta_{33}$  are shown in Fig. 6. We shall hereafter consider only the influence of pressure on the parameters

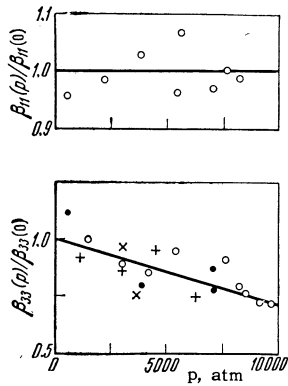


FIG. 6. The Sb coefficients  $\beta_{11}$  and  $\beta_{33}$  versus pressure.

of the electron Fermi surface, since no generally accepted model of the hole surface exists.

## 6. CALCULATION OF PRESSURE DEPENDENCE OF THE ELECTRONIC PARAMETERS

The six galvanomagnetic coefficients  $B_{24}$ ,  $B_{42}$ ,  $B_{33}$ ,  $B_{11}$ ,  $\beta_{33}$ , and  $\beta_{11}$  are given in terms of the parameters of the electron Fermi surface as follows:

$$\begin{aligned}
 B_{33} &= (ne/c^2)a^2b^2\mu_1(\mu_3 - \mu_2)^2, \\
 B_{11} &= (ne/8c^2)[a^2\mu_2(\mu_1 - \mu_3)^2 \\
 &\quad + b^2\mu_3(\mu_1 - \mu_2)^2 + 3a^2b^2\mu_1(\mu_3 - \mu_2)^2], \\
 B_{42} &= (ne/4c^2)ab(\mu_3 - \mu_2)(a^2\mu_1\mu_2 + b^2\mu_1\mu_3 - \mu_2\mu_3), \\
 B_{24} &= (ne/4c^2)ab(\mu_3 - \mu_2)(\mu_1 - a^2\mu_3 - b^2\mu_2), \\
 \beta_{33} &= \mu_1(a^2\mu_3 + b^2\mu_2)/c^2, \\
 \beta_{11} &= [3\mu_1(a^2\mu_2 + b^2\mu_3) + \mu_2\mu_3]/c^2. \quad (4)
 \end{aligned}$$

Here  $c$  is the velocity of light,  $e$  is the electronic charge,  $\mu_i$  are the mobility tensor components along the principal axes of the ellipsoid,  $n$  is the carrier density,  $a = \sin \theta$ , and  $b = \cos \theta$  (where  $\theta$  is the rotation angle of the ellipsoid around the trigonal axis).

Because of the relation (3), five independent equations exist for determining the five electron parameters  $\mu_1$ ,  $\mu_2$ ,  $\mu_3$ ,  $\theta$ , and  $n$ . The algebraic solution of this system of equations is given in the Appendix. The absolute parameters determined in this way are insufficiently reliable, because they represent differences between two large numbers (see the expression for  $\gamma_4^2$  in the Appendix), and are strongly affected by the spread of the experimental galvanomagnetic coefficients.<sup>3)</sup> However, the

<sup>3)</sup>Zitter has pointed out the analogous instability of the solutions for Bi.<sup>[15]</sup>

pressure dependence of the spectral parameters is less sensitive to this instability and is determined essentially by the pressure dependence of the galvanomagnetic coefficients rather than by the absolute values of the latter.

Columns 4–8 of Table III give, in relative units, the pressure dependences of the electron parameters  $\mu_1$ ,  $\mu_2$ ,  $\mu_3$ ,  $\theta$ , and  $n$  up to 10 000 atm. However, it must be remembered that in this calculation since the absolute value of  $\mu_2$  is small its pressure dependence is subject to the greatest error.

Data on cyclotron resonance and other effects in<sup>[4-6]</sup> show that  $m_2 \gg m_1$ ,  $m_3$ . Since large anisotropy of the relaxation time is not expected in Sb, this inequality is apparently maintained for the mobilities and  $\mu_2 \ll \mu_1$ ,  $\mu_3$ . Therefore an approximate solution of the system (4) can be obtained by setting  $\mu_2 = 0$ . In this case the expressions for the parameters are simplified and their pressure dependences are derived explicitly from the pressure dependences of the conductivity tensor components (see the Appendix). The number of required parameters is reduced to four, so that one of the equations can be used to check the correctness of the solution.

We take as our initial terms those components of the conductivity tensor that are clearly determined from the parameters of the electron Fermi surface ( $B_{33}$ ,  $\beta_{33}$ ,  $B_{42}$ , and  $B_{24}$ ). Columns 9–12 of Table III give the calculated pressure dependences of  $\mu_1$ ,  $\mu_3$ ,  $\theta$ , and  $n$ ; columns 13 and 14 give, as a check, the pressure dependences of  $B_{11}$  and  $\beta_{11}$  that were calculated therefrom. The good agreement with experiment (see columns 2 and 3 of Table III) is further evidence that the longitudinal magnetoresistance along the binary axis depends only on the parameters of the electron Fermi surface.

## 7. CONCLUSION

When the results of the two variants of the calculation are compared we find that the pressure dependences of  $\mu_1$ ,  $\mu_3$ , and  $\tan \theta$  have been determined relatively reliably, while the pressure dependences of  $\mu_2$  and  $n$  are subject to large errors. In any event, these calculations furnish a qualitative picture of the pressure dependence of the electron Fermi surface for Sb.

Figure 7 shows the dependence of the electron parameters on the ratio  $c/a$  and on pressure up to 10 000 atm for solution I. It is seen that  $\mu_1$  increases slightly,  $\mu_3$  decreases slightly, and  $\mu_2$  is subject to a relatively large decrease. If we neglect the pressure dependence of the relaxation time  $\tau_i$ , we can use the pressure dependence of  $\mu_i$  to evalu-

Table III. Pressure dependence of relative parameters of Sb electron Fermi surface

p, atm	Experimental		Solution I ( $\mu_2 \neq 0$ )					Solution II ( $\mu_2 = 0$ )					
	$B_{11}(p)$	$\beta_{11}(p)$	$\mu_1(p)$	$\mu_2(p)$	$\mu_3(p)$	$\tan \theta(p)$	$n(p)$	$\mu_1(p)$	$\mu_2(p)$	$\tan \theta(p)$	$n(p)$	$B_{11}(p)$	$\beta_{11}(p)$
	$B_{11}(0)$	$\beta_{11}(0)$	$\mu_1(0)$	$\mu_2(0)$	$\mu_3(0)$	$\tan \theta(0)$	$n(0)$	$\mu_1(0)$	$\mu_2(0)$	$\tan \theta(0)$	$n(0)$	$B_{11}(0)$	$\beta_{11}(0)$
1	2	3	4	5	6	7	8	9	10	11	12	13	14
1	1.000	1.000	1.000	1.000	1.000	1.000	1.000	1.000	1.000	1.000	1.000	1.000	1.000
2000	0.952	1.000	1.011	0.921	0.996	0.964	0.889	1.003	0.986	0.975	0.972	0.951	0.993
4000	0.904	1.000	1.021	0.849	0.991	0.945	0.801	1.011	0.969	0.947	0.941	0.904	0.990
6000	0.856	1.000	1.028	0.781	0.987	0.915	0.715	1.023	0.957	0.915	0.899	0.854	0.995
8000	0.808	1.000	1.035	0.722	0.982	0.874	0.650	1.039	0.953	0.875	0.841	0.799	1.014
10000	0.760	1.000	1.038	0.671	0.978	0.826	0.595	1.060	0.960	0.827	0.764	0.740	1.052

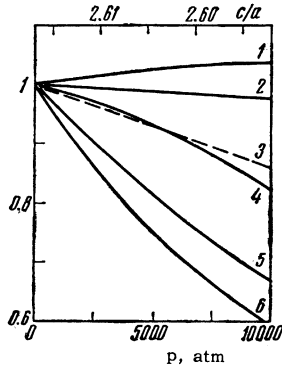


FIG. 7. Parameters of the electron Fermi surface of Sb versus pressure and  $c/a$ . 1 -  $\mu_1$ ; 2 -  $\mu_3$ ; 3 -  $\tan(60^\circ - \alpha)$ , where  $\alpha$  is the rhombohedral angle; 4 -  $\tan \theta$ ; 5 -  $\mu_2$ ; 6 -  $n$ .

ate the pressure dependence of the effective mass. For Sb the effective mass ratios are  $m_1 : m_2 : m_3 = 1 : 28.8 : 1.34$ ; [5] at 10 000 atm these ratios become  $1 : 44.5 : 1.42$ . The electron ellipsoids are therefore greatly extended in the directions of their long axes (as in [8]). The number of carriers is reduced by 20–40%; this follows qualitatively from the fact that all conductivity tensor components, without exception, decrease at higher pressures.

It must be mentioned that the carrier density also decreases in Bi with increasing pressure. [8] Figure 8 represents an electron ellipsoid of Sb

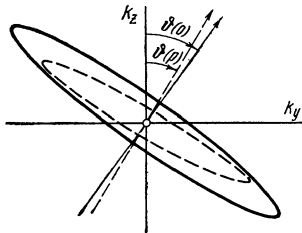


FIG. 8. Deformation of the electron Fermi surface of Sb under pressure according to solution I in Table III. The scale of the long ellipsoidal axis has been reduced by a factor of three. The continuous ellipsoid pertains to 1 atm; the dashed ellipsoid pertains to 10 000 atm.

plotted with respect to the crystallographic axes for 1 atm and 10 000 atm according to solution I of Table III.

The most interesting result is the decreasing tilt of the ellipsoid under increasing pressure. This effect can be associated with direct experimental data, since for  $\mu_2 = 0$  we obtain  $\tan \theta = B_{33}/4B_{42} = (3\beta_{33}/4\beta_{11})^{1/2}$ .

Figure 9 shows the pressure dependence of  $B_{33}/4B_{42} = A_{33}\rho_{11}/4\rho_{33}A_{42}$ ; in this connection it is important to note that  $A_{33}$  and  $A_{42}$  were obtained for the same samples. Figure 7 also shows the pressure dependence of  $\tan(60^\circ - \alpha)$  for Sb, and the almost identical dependence of  $\tan \theta$ .

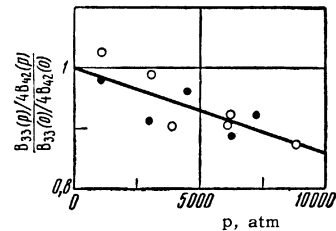


FIG. 9. Pressure dependence of  $(B_{33}/4B_{42}) \approx \tan \theta$ .

The x-ray patterns obtained in [9] show that at 70 000 atm Sb has a simple cubic structure. It has been shown in [16] on the basis of simple considerations that Sb with this structure should have the same carrier density as a normal metal. The energy spectrum of a normal metal cannot be derived from the known spectrum of Sb (which has a low carrier density) by gradually changing the latter, especially since our work has shown that the carrier density decreases appreciably up to 10 000 atm. To account for the transformation we must continue the measurements up to more than 30 000 atm, where, as Bridgman has shown, [17] the resistance is considerably reduced.

At the present time the shape of the hole Fermi surface of Sb is being discussed vigorously on the basis of new measurements. We hope that in the

near future we shall have a complete picture of the pressure dependence of the Sb Fermi surface based on the measurements described here.

The authors wish to thank L. F. Vereshchagin for his continued interest, and R. G. Arkhipov and S. S. Kabalkin for valuable discussions.

#### APPENDIX

The solution of (4) can be obtained most easily in terms of the mobility tensor components using coordinates associated with the crystallographic axes:

$$\gamma_i = \begin{pmatrix} \gamma_1 & 0 & 0 \\ 0 & \gamma_2 & \gamma_4 \\ 0 & \gamma_4 & \gamma_3 \end{pmatrix} \quad (5)$$

Since the equations of (4) are subject to the relation (3), we select the following five basic coefficients:  $B_{33}$ ,  $B_{11}$ ,  $B_{42}$ ,  $\beta_{33}$ , and  $\beta_{11}$ . For  $\gamma_i$  and the density  $n$  we then easily obtain

$$\begin{aligned} \gamma_1 &= c[(\beta_{11}B_4 - \beta_{33}B_1) / (3B_1 - 4)]^{1/2}, & \gamma_2 &= c^2\beta_{33} / \gamma_1, \\ \gamma_3 &= [(4B_1 - 5)\gamma_1 + \gamma_2] / B_4, \\ \gamma_4^2 &= (3\gamma_1 + \gamma_2)\gamma_3 - 4c^2\beta_{11}, \\ n &= c^2B_{33} / e\gamma_1\gamma_4^2; \end{aligned} \quad (II.1)$$

where

$$B_1 = 2B_{11} / B_{33}, \quad B_4 = [B_{33}(B_1 - 1) / B_{42}]^2. \quad (6)$$

We have the following relations to the mobility tensor components in the ellipsoidal principal axes:

$$\begin{aligned} \mu_1 &= \gamma_1, & \mu_{2,3} &= 1/2\{(\gamma_2 + \gamma_3) \pm [(\gamma_3 - \gamma_1)^2 + 4\gamma_4^2]^{1/2}\}; \\ \text{tg } 2\theta &= 2\gamma_4 / (\gamma_3 - \gamma_2). \end{aligned} \quad (II.2)^*$$

We note that the solutions in the  $\gamma$  representation (II.1) are unique if the mobilities are defined as positive (as is customary). The solutions (II.2) are not unique, as can be seen from the equations of (4), since the latter are invariant with respect to the simultaneous substitutions  $\mu_2 \rightleftharpoons \mu_3$  and  $\theta \rightarrow (\pi/2 - \theta)$ . This invariance belongs in general to all equations for  $\sigma_{ij}$ ,  $P_{ijk}$ , and  $B_{ij}$ . For this reason the assumption  $\mu_2 = 0$  not only simplifies the equations, but also leads to what we may call the "physical solution" of the equations containing  $\mu_i$ . In this approximation we obtain immediately

$$\begin{aligned} \text{tg } \theta &= (3\beta_{33} / 4\beta_{11})^{1/2} \equiv B_{33} / 4B_{42}, \\ \mu_1 &= cB_0\beta_{33}^{1/2}, \\ \mu_3 &= c(3\beta_{33} + 4\beta_{11}) / 3B_0, \\ n &= 3B_{33}B_0 / 4ec\beta_{11}(\beta_{33})^{1/2}, \\ B_0 &= (8B_{11} / B_{33} - 3)^{1/2}. \end{aligned} \quad (II.3)$$

Thus, in the approximation  $\mu_2 = 0$ , the relative

pressure dependence of  $\tan \theta$  depends exclusively on the relative dependences of the galvanomagnetic coefficients. The other parameters, taking  $3\beta_{33} + 4\beta_{11} \approx 4\beta_{11} \sec^2 \theta$ , depend on the absolute galvanomagnetic coefficients only through the expression  $(8B_{11}/B_{33} - 3)^{1/2}$ . If  $\pm 20\%$  accuracy of the absolute values of  $B_{11}$  and  $B_{33}$  is assumed, at 10 000 atm this factor leads to at most  $\pm 2\%$  uncertainty for  $\mu_1$ ,  $\mu_3$ , and  $n$ .

It should also be noted that the galvanomagnetic coefficients  $B_{24}$  and  $B_{42}$  critically affect the sign of the angle  $\theta$ . Negative values of these coefficients indicate that the ellipsoids have been rotated in the direction opposite to the case for Bi.

<sup>1</sup>R. G. Arkhipov, JETP **43**, 349 (1962), Soviet Phys. JETP **16**, 251 (1963).

<sup>2</sup>A. A. Abrikosov and L. A. Fal'kovskii, JETP **43**, 1090 (1962), Soviet Phys. JETP **16**, 769 (1963).

<sup>3</sup>Barrett, Cucka, and Haefner, Acta Cryst. **16**, 451 (1963).

<sup>4</sup>Brandt, Dolgolenko, and Stupochenko, JETP **45**, 1319 (1963), Soviet Phys. JETP **18**, 908 (1963).

<sup>5</sup>D. Shoenberg, Phil. Trans. Roy. Soc. London **A245**, 1 (1952); W. R. Datars, Can. J. Phys. **40**, 1784 (1962); Y. Eckstein, Phys. Rev. **129**, 12 (1963); J. Ketterson, Phys. Rev. **129**, 18 (1963); J. Ketterson and Y. Eckstein, Phys. Rev. **132**, 1885 (1964).

<sup>6</sup>Rao, Zebouni, Grenier, and Reynolds, Phys. Rev. **133**, A141 (1964).

<sup>7</sup>P. W. Bridgman, The Physics of High Pressure, Bell, London, 1931 (Russ. transl., ONTI, M.-L., 1935).

<sup>8</sup>S. S. Sekoyan and A. I. Likhter, FTT **2**, 1940 (1960), Soviet Phys.-Solid State **2**, 1748 (1960); N. B. Brandt and V. A. Ventsel', JETP **35**, 1083 (1958), Soviet Phys. JETP **8**, 757 (1959).

<sup>9</sup>L. F. Vereshchagin and S. S. Kabalkina, JETP **47**, 414 (1964), Soviet Phys. JETP **20**, 274 (1965).

<sup>10</sup>A. I. Likhter and V. V. Kechin, FTT **5**, 3066 (1963), Soviet Phys. Solid State **5**, 2246 (1963).

<sup>11</sup>H. J. Juretschke, Acta. Cryst. **8**, 716 (1955).

<sup>12</sup>S. J. Freedman and H. J. Juretschke, Phys. Rev. **124**, 1379 (1961).

<sup>13</sup>S. Epstein and H. J. Juretschke, Phys. Rev. **129**, 1148 (1963).

<sup>14</sup>Yu. A. Pospelov and V. V. Kechin, FTT **6**, 3206 (1964), Soviet Phys. Solid State **6**,

<sup>15</sup>R. N. Zitter, Phys. Rev. **127**, 1471 (1962).

<sup>16</sup>J. M. Luttinger, Phys. Rev. **119**, 1153 (1960).

<sup>17</sup>P. W. Bridgman, Proc. Am. Acad. Arts Sci. **81**, 169 (1952).

Translated by I. Emin